JAAS

Accuracy improvement in XRF analysis for the quantification of elements ranging from tenths to thousands µg/g in human tissues using different matrix reference materials

Journal:	*Journal of Analytical Atomic Spectrometry*
Manuscript ID	JA-ART-07-2020-000307.R2
Article Type:	Paper
Date Submitted by the Author:	n/a
Complete List of Authors:	Machado, Jorge; LIBPhys-UNL, Laboratory for Instrumentation, Biomedical Engineering and Radiation Physics, and Departamento de Física da Faculdade de Ciências e Tecnologia, Universidade Nova de Lisboa, 2829-516 Caparica, Physics da Silva Carvalho, Patrícia; LIBPhys-UNL, Laboratory for Instrumentation, Biomedical Engineering and Radiation Physics, and Departamento de Física da Faculdade de Ciências e Tecnologia, Universidade Nova de Lisboa, 2829-516 Caparica, Physics Félix, Ana; Universidade Nova de Lisboa Faculdade de Ciencias Medicas, Pathology; Instituto Portugues de Oncologia de Lisboa Francisco Gentil EPE, Pathology Doutel, Delfin; Instituto Portugues de Oncologia de Lisboa Francisco Gentil EPE, Pathology Santos, José Paulo; Centro de Física Atómica (CFA/FCUL), Departamento de Física, Faculdade de Ciências e Tecnologia, FCT, Universidade Nova de Lisboa, Physics Carvalho, Maria; Centro de Fisica Atomica da Universidade de Lisboa, Faculdade de Ciencias Pessanha, Sofia; LIBPhys-UNL, Laboratory for Instrumentation, Biomedical Engineering and Radiation Physics, and Departamento de Física da Faculdade de Ciências e Tecnologia, Universidade Nova de Lisboa, 2829-516 Caparica, Physics

JAAS
Journal of Analytical Atomic Spectrometry

Guidelines for Referees

Thank you very much for agreeing to review this manuscript for *Journal of Analytical Atomic Spectrometry* (*JAAS*)

JAAS is the central journal for publishing innovative research on fundamentals, instrumentation, and methods in the determination, speciation and isotopic analysis of (trace) elements within all fields of application. This includes, but is not restricted to, the most recent progress, developments and achievements in all forms of atomic and elemental detection, isotope ratio determination, molecular analysis, plasma-based analysis and X-ray techniques.

JAAS' Impact Factor is **3.646** (2018 Journal Citation Reports®)

The following manuscript has been submitted for consideration as a

FULL PAPER

Full papers must represent a significant development in the particular field of analysis and are judged according to originality, quality of scientific content and contribution to existing knowledge. Although there is no page limit for Full papers, appropriateness of length to content of new science will be taken into consideration.

Please consider these standards when making your recommendation for publication in *JAAS*:

- Use the **journal scope and expectations** to assess the manuscript's suitability for publication in *JAAS*.
- **Comment on** the originality, importance, impact and reliability of the science. English language and grammatical errors do not need to be discussed in detail, except where it impedes scientific understanding.
- **Note that routine or incremental** work should not be recommended for publication.
- Check for an accompanying '**Significance to *JAAS***' statement
- **Contact the Editorial Office** if there is any conflict of interest, if the work has been previously published or if there is a significant part of the work which you are not able to referee with confidence.

Best regards,

Professor Martin Resano
Chair, *JAAS*

Philippa Ross
Executive Editor, *JAAS*

Contact us

Please visit our reviewer hub for further details of our processes, policies and reviewer responsibilities as well as guidance on how to review, or click the links below.

What to do when you review

Reviewer responsibilities

Process & policies

Accuracy improvement in XRF analysis for the quantification of elements ranging from tenths to thousands µg/g in human tissues using different matrix reference materials

Jorge Machado[1], Patrícia Miguel Carvalho[1], Ana Félix[2,3], Delfin Doutel[3], José Paulo Santos[1], Maria Luísa Carvalho[1], Sofia Pessanha[1]

[1]Laboratory of Instrumentation, Biomedical Engineering and Radiation Physics, NOVA School of Science and Technology, Campus Caparica, 2829-516, Monte Caparica, Portugal

[2] NOVA Medical School, Campo Mártires da Pátria 130, 1169-056 Lisbon, Portugal

[3] Serviço de Anatomia Patológica, Instituto Português de Oncologia de Lisboa Francisco Gentil, IPOLFG, R. Prof. Lima Basto, 1099-025, Lisbon, Portugal

Abstract

In this work, we aim at achieving the most accurate quantitative determination of elements in human tissues by means of X-ray Fluorescence spectrometry using the external calibration approach. A calibration curve built using a set of certified reference materials (CRM) of animal tissue was compared with the one obtained with a set of CRMs of plants and leaves with lower atomic number Z but with correction of the matrix using the scattering peaks of the X-ray tube anode. Finally, a calibration curve combining the two sets of CRMs was built and the accuracy of the quantification using the three methods was compared and a more precise method of quantification was obtained. This improved approach was tested on five paired samples of normal and tumour human tissue. Despite the high heterogeneity of the samples, and given the improvement in accuracy of the measurements, significant differences were found in the elemental concentration of low-Z elements.

1. Introduction

Quantitative determinations in Energy Dispersive X-ray Fluorescence (EDXRF) spectrometry require the use of suitable empirical and/or theoretical methods in order to convert the fluorescent intensities of the spectra into the concentration of the analyte [1]. Apart from infinitely thin samples, this conversion is not straightforward as the measured intensities are strongly influenced by the surrounding elements of the sample, or matrix, resulting in absorption and enhancement effects. The most popular quantification method used in EDXRF

is the Fundamental Parameter method (FP). It is based on mathematical equations initially derived by Sherman in 1955 [2] and corrected by Shiraiwa and Fujino in 1966 [1]. This method estimates a composition for the unknown sample by calculating the theoretical fluorescence intensities and iteratively comparing them with the measured ones, until a correspondence is obtained [3]. Additionally, the FP approach can take advantage of certified reference materials (CRM), and an analysis employing a CRM of similar composition as the unknown material will give better results than by using a very different CRM. Pascolo et al. [4] used bovine liver SRM 1577B for calibration of the X-ray Fluorescence spectra to compare quantitative determinations on fresh and frozen–thawed human ovarian tissues using synchrotron radiation.

The accuracy of these determinations relies on many factors, namely, the knowledge of the spectral distribution of the excitation radiation [5] and the estimation of the matrix composition. This can be difficult to achieve when applying polychromatic excitation using focusing optics on the study of samples with dark matrix, such as human tissues. A reliable alternative could be the use of external standard calibration curves for the assessment of essential and trace elements (e.g., potassium, calcium, manganese, and iron). This method consists of determining the concentration of an unknown specimen by comparing its fluorescence intensity with the one of an accurately known specimen. Such comparisons are only justified if the fluorescent element is associated with a uniform matrix retrieving a smooth calibration curve of intensity as a function of concentration[3] [6]. These calibrations involve the use of certified reference materials with known concentrations and similar matrices, which can be used to build models for the purpose of quantifying photon intensities in XRF spectra.

This approach was also used by Banas et al.[7] and Kwiatek et al.[8] for the determination of the concentrations of Mn, Fe, Cu, and Zn and their correlations with the clinical stage of the prostate cancer, using two homemade standards, prepared using N,N′-methylenebisacrylamide mixed with different aqueous solutions of metal nitrates.

Geraki et al.[9], Poletti et al.[10], and Farquharson et al.[11] also used the external standard quantification approach to study the K, Ca, Mn, Fe, Cu, and Zn concentrations in breast tissues by means of calibration curves constructed with reference water solutions of known concentrations in order to simulate the matrix effects of healthy tissues as well as of neoplastic ones. The methodology was further improved by Silva et al. [12] that used the scattered radiation in each XRF spectrum to correct the calibration curve and improve accuracy of the quantification of normal and neoplastic breast tissue.

Abnet et al.[13] also used CRMs with different matrix compositions, NIST 1832 and 1833 SRM (Thin Glass Film on Polycarbonate), to quantify Zn, Fe, Cu, and Ni concentrations in 5 μm

thick oesophageal biopsy specimens by taking into account photoelectric absorption cross sections based on fluorescence yields, absorption by the beryllium window of the energy-dispersive fluorescence detector, and absorption by a dead layer on the detector.

However, the quantification of trace elements using calibration curves from sets of certified reference materials (CRMs) has several known limitations, mainly scarcity of suitable CRMs. This concerns both the amount of CRM available, rendering curves with poor statistics and high uncertainty, as well as the small concentration range for certain elements through the set of CRMs of the same matrix. Having a small range of concentrations in the calibration curve may increase the uncertainty in the quantification of an unknown sample, especially when the concentration is obtained by extrapolation of the calibration curve.

In this work, we aimed at improving the accuracy of quantitative determinations of elements present in human tissues by X-ray Fluorescence spectrometry, using the external calibration approach. Through the combination of two sets with low, yet similar, mean-*Z* CRMs with different matrices and the correction of the matrix effects using the scattering peaks of the X-ray tube anode, we could increase both the number of points and the elemental concentration range in the calibration curves. The obtained curve was employed in the quantification of unknown paired samples of tumour and normal human tissues, to assess concentration variations between them.

2. Material and methods

2.1. Experimental setup

The μ-EDXRF system consisted in the M4 Tornado – Bruker (Germany). The X-ray tube is a micro-focus side window low-power rhodium tube, operated at 50 kV and 300 μA. A polycapillary lens was used to obtain a spot size down to 25 μm for Mo-Kα. No filters were used during acquisition. Detection of fluorescence radiation was performed by an energy dispersive silicon drift detector with 30 mm^2 sensitive area and energy resolution of 142 eV for Mn-Kα. To guarantee that the analysis was the most representative as possible of the average composition of the CRMs, area acquisition was performed, instead of spot analysis. This way, the sum spectrum of all the analysed area was considered. Mappings were performed in 3 different 10 x 10 mm^2 areas, using a step size of 35 μm and time per step of 12 ms/pixel over 1 cycle, rendering a total acquisition time of 840 s.

The analysis of the unknown samples was performed under the same experimental conditions as the CRMs. Instead of area mappings, for each sample 15 spot analysis were randomly selected, for the duration of 300 s.

2.2. Certified Reference Materials (CRM)

In order to build calibration curves for the external standard method of quantification, 15 animal and plant CRMs were used: NIST SRM 1577a Bovine Liver, NIST SRM 1566 Oyster Tissue, IAEA MA-A-2 Fish Flesh Homogenate, NRC-CNRC TORT-2 Lobster Hepatopancreas Reference Material for Trace Metals, ERM-BB186 Pig Kidney, ERM-BB184 Bovine Muscle, BCR-185R Bovine Liver, NRC – CNRC DORM-4 Fish Protein certified reference material for trace metals, INCT-OBTL-5 Oriental Basma Tobacco Leaves, NIST SRM 1571 Orchard Leaves, GBW 07603 Trace Elements in Bush Branches and Leaves, GBW 07604 Poplar Leaves, GBW 07605 Tea, NIST SRM 1575 Pine Needles, and IAEA-336 Trace and Minor Elements in Lichen.

All CRMs were analysed as 15 mm diameter and 1 mm thick pressed pellets, glued on a Mylar film, and placed on a sample holder directly under the X-ray beam. A comparison of the obtained spectra for reference materials NIST SRM 1566 Oyster Tissue and NIST SRM 1571 Orchard Leaves is presented in the supplementary material (Fig.S1). As can be seen, the elemental composition is different between CRMs, but the background and scattering peaks are very similar.

2.3. Human tissue samples

For this study, a total of five patients diagnosed with tumour pathology and followed at the Instituto Português de Oncologia de Lisboa Francisco Gentil Lisboa (IPOLFG) were randomly selected. The patients were all female, with ages ranging from 47 to 75 years old; three were diagnosed with high-grade carcinomas of the endometrium and two, with invasive breast carcinoma. More detailed information can be consulted in table 1.

From each case, tumour and adjacent normal tissues were collected from surgical procedures at IPOLFG and underwent histopathological analysis for diagnosis. Then, five sets of paired samples for EDXRF analysis were prepared, by freezing each tissue with isopentane.

At the LIBPhys laboratory at NOVA School of Science and Technology, the samples were prepared for analysis: first, they were thawed at room temperature and then freeze-dried for a period of 17 hours.

Heterogeneity of samples, especially human tissue, can be a source of large systematic errors (up to 50%) due to particle size and surface effects that particularly influence the line intensities of low-Z elements. Ideally, these errors are minimized by adequate preparations methods, such as sample powdering followed by preparation of pressed pellets, that ensure a homogeneous sample with a smooth surface and small enough grains[14]. Due to the low

amount of available tissue it was not possible to make pellets and therefore the unknowns were analysed as is.

This constraint is inherent to the analysis of human tissue, as the available biopsied tissue will always be limited. This way, using the external standard approach with compensation with the scattered radiation of the characteristic lines of the X-ray tube, will compensate for particle size, surface texture effects and packing density[6,15].

Moreover, the influence of sample thickness on the proposed quantification method was assessed. All the samples were measured using a calliper rule and it was concluded that they are not infinitely thick for the Compton-to-Rayleigh ratios to be independent of the thickness. However, all the samples present the same thickness, ~1 mm, apart from sample B02 normal, which is thicker, ~3 mm. For this sample, the variation of the Compton-to-Rayleigh ratio was evaluated using the attenuation coefficients of ICRU four component soft tissue (National Institute of Standards and Technology – NIST, database), for the Rh energy. It was found that this variation is negligible, when compared with the uncertainty due to the inhomogeneity of the sample and has virtually no effect on the elemental quantification uncertainty. For example, the obtained final uncertainty in the quantification of Zn for the B02 normal sample when considering the influence of the sample thickness was found to be only 4% higher.

2.4. Spectra analysis

All data was analysed using the advanced spectra processing tools of ROOT[16]. All peaks present in the spectra were identified and the background estimated using the method based on the Sensitive Nonlinear Iterative Peak (SNIP) clipping algorithm[17]. A fit function composed of a sum of gaussian functions was then fitted to the spectra by χ^2 minimization techniques. The number of gaussians of the fit function correspond to the number of the found peaks, i.e., the characteristic X-ray fluorescence peaks of each element present in the sample, and the dispersion peaks. Each peak was numerically integrated with the respective uncertainty due to the fit. Fig. 1 shows an example of the analysis procedure, applied to one spectrum of the sample U02.

2.5. Statistical analysis

Statistical analysis was performed with OriginPro 2016. Firstly, Shapiro-Wilk test for normality distribution evaluation was performed[18]. Considering all the variables tested, Wilcoxon Sign rank test, a non-parametric paired sample test was used in order to compare the results obtained for tumour and adjacent normal tissues, and examine if there are differences in the concentrations of elements, considering a significance level of 0.05[19].

3. Quantification methodology

3.1 Mean-*Z* model

This work was developed under the premise that by using two sets of CRMs with different matrices, yet similar low mean-*Z,* the accuracy in the quantification of elements with the external calibration method can be improved.

In order to verify how close the mean-*Z* values of the different sets of CRMs are, we experimentally obtained a dependency model of the mean-*Z* as a function of the Compton-to-Rayleigh ratio. A set of samples consisting of different proportions of reference materials of HAp [$Ca_{10}(PO_4)_6(OH)_2$] (Sigma-Aldrich, lot #BCBS8492V), and boric acid [H_3BO_3] (for conservation–restoration purposes) was created in order to obtain an average atomic number range of $7 < Z < 14$. The average atomic number, Z_i, of each material has been calculated according to expression (1):

$$\overline{Z} = \sum_i w_i Z_i$$

with w_i, the mass fraction, and Z_i, the atomic number of the element i. The list of model samples with corresponding $\overline{Z}$ is presented in Pessanha et al. [20]

The intensity ratio as a function of the calculated mean-*Z* is shown in Fig. 2. Different models were applied to the experimental values, and the ones that better describe the data are shown in Fig. 2. From the parameterized model, represented by the blue curve, and from the experimental determination of the Compton-to-Rayleigh ratio of all samples, the mean-*Z* of the two CRM sets was calculated. As it can be seen, the mean-*Z* values of all CRMs are in the interval between 6.1 and 7.3, which means that the largest difference in mean-*Z* of all used CRMs is around 1.2.

3.2. Calibration curves

From the acquired spectra of CRMs described in section 2.2, we built calibration curves of the concentration of a given element in the sample as a function of the Kα peak integral divided by the Compton-to-Rayleigh ratio, for the different elements, by fitting the data with a linear regression, weighted by the error bars of each point. Moreover, 3 different curves for each element were constructed in order to compare the calibration curves of the two different sets of CRMs and to test the theory that the addition of the plant CRMs improves the accuracy and statistical significance of the model in all range of available data. Figs. 3 to 5 present, respectively, the calibration curves for Fe, S and K. The error bars associated to the points represent the concentration uncertainty of each certified value, and the maximum deviation

of the respective peak intensity divided by the Compton-to-Rayleigh ratio from 3 different measurements, quadratically combined with the uncertainty due to the fit. The shaded area in the figures represents the 1σ confidence interval of each fit to the three different data sets: the first considering only the plant CRMs, the second considering only the animal tissue CRMs, and the third considering both CRM sets. As it can be seen from Figs. 3 and 5, the cases of Fe and K, if we have similar elemental concentration ranges, the calibration curves are identical, yet when all points are considered, the 1σ confidence interval is narrower due to the increased number of points in the model. Thus, this shows that we can improve the uncertainty in the quantification of animal tissue samples by combining these two sets of CRMs with similar mean atomic number. In the case of S, shown in Fig. 4, the situation is very different. Only two animal tissue CRMs are available containing certified concentration values and both with very similar concentration values. Therefore, we can only quantify a given sample when we also have a similar K concentration, otherwise if we quantify a value outside of the range delimited by the two points, the uncertainty in the quantification by extrapolation of the curve will be enormous, as it can be seen by the confidence interval of the fit represented by the red shaded area. By including the plant CRMs in the calibration curve, the problem is overcome. Hence, the addition of plant CRMs in the calibration curve significantly improves the fit and increases the range of concentration for which we can apply this calibration curve to quantify K in animal tissue, with significantly lower uncertainty.

The linear regression coefficients of the Fe, K, and S calibration curves, and the coefficients for the remaining elements are presented in Table 2, as well as the significance of the obtained slope, determined as multiples of the standard error. This way, the significance of the slope value can be used to evaluate the accuracy of each calibration curve. As can be seen from the table, less accurate values are obtained using only animal tissue CRMs for the quantification of elements from P to Mn, because of the small concentration range of the set. For the same reason, the curve obtained using only the plant CRMs is less accurate for elements with higher Z, Cu and Zn. As expected, the combination of both sets of CRMs, rendered higher significance for all elements. This is illustrated by the standard error values associated with each coefficient of the linear regression. In some cases, when using only one set of CRMs, the standard error value is larger than the value itself (e.g., S calibration curve using only animal tissues). However, this is never the case, when the linear regression is built by the combination of both sets.

To further assess the accuracy of the method, the calibration curves for animal tissues and all tissues were applied to CRM - NIST SRM 1577a Bovine Liver. Table 3 presents the obtained

concentrations and the relative difference to the certified value. As can be seen, both the relative difference and the uncertainty of the value decreased when all CRM were used.

3.3. Limits of detection (LoD) and quantification (LoQ)

We have calculated the Limit of Detection (LoD) and the Limit of Quantification (LoQ) of each studied element, by using the calibration curves with both CRM sets. The calculation was done by determining the residual standard error of the linear regressions; according to equation (2)[21], the LoD is:

$$LoD = \delta_{\alpha,\beta,\nu} \cdot \frac{Sr}{\hat{b}} \left[1 + \frac{1}{n} + \frac{\bar{x}^2}{Sxx}\right]^{\frac{1}{2}},$$

where $\hat{b}$ represents the slope of the linear regression; *n,* the number of points in the calibration curve; and $\bar{x}$, the mean value of the concentration. The variables Sr and Sxx represent the residual standard error and the sum of difference, respectively, and are expressed as:

$$Sr = \sqrt{\frac{\sum_{i=1}^{n}(y_i - \hat{y}_i)^2}{\nu}} \quad ; \quad Sxx = \sum_{i=1}^{n}(x_i - \bar{x})^2.$$

$\delta_{\alpha,\beta,\nu}$ is the value of the noncentrality parameter of the noncentral *t*-distribution with $\nu = n - 2$ degrees of freedom[22]. For large ν and α=β, a good approximation is given by

$$\delta_{\alpha,\beta,\nu} \approx 2t_{1-\alpha}(\nu),$$

where $2t_{1-\alpha}(\nu)$ is the (1-α)-quantile of the *t*-distribution with ν degrees of freedom.

Table 4 shows the LoD and LoQ for every studied element. The LoQ has been calculated considering that LoQ ≈ 3LoD [21].

4. Results and Discussion

In this section, we discuss the application of the described method to the 5 paired human tissue samples, discussed in sec. 2.3. For each sample, we have measured and analysed 15 different points using the same spectral analysis procedure as for the CRM spectra. From the 15 measurements, we have taken as the value for the intensity of a given characteristic X-ray peak divided by the respective Compton-to-Rayleigh ratio, the average of the 15 measurements, and the standard deviation as the uncertainty.

Figs. 6 and 7 present the comparison of the mean elemental concentrations and standard deviation for tissue samples U02 and B01 respectively. The error bars are, in some cases, quite large, depicting the heterogeneity of the samples regarding some elements, namely Ca and Fe. Significant differences determined by Wilcoxon Sign rank test are presented with p-value. The elemental concentrations for the remaining tissues, U01, U03 and B02 are presented in supplementary material (Fig.S2-S4)

As can be seen, from the analysis of the elemental composition of normal breast tissue, the obtained order of magnitude is in compliance with the elemental concentrations determined in breast tissue using other destructive and matrix independent elemental techniques, where values for P ranging from 586 to 2500 ug.g^{-1}, for S ranging from 800 to 900 ug.g^{-1}, for K ranging from 486 to 2400 ug.g^{-1}, for Fe ranging from 23 to 57 ug.g^{-1}, and for Zn ranging from 6 to 36 ug.g^{-1} were obtained[23–25]. Sample B01 was also analysed destructively using Inductively Coupled Plasma – Atomic Emission Spectroscopy (ICP-AES) and the results are within the obtained order of magnitude for elements P, K and Zn (Fig.S5). Although the available literature for elemental determinations in uterus is scarce compared to breast, the obtained values for Zn and Fe are also in accordance with the ones obtained by Nasiadek et al.[26] Additionally, when comparing both types of tissue, it is visible that breast and uterus have different concentration of lighter elements with the concentration of P, S, and K over 1000 µg.g^{-1} in uterine samples. Additionally, the presence of Ca only in tissue U02 is striking, it is common to find crystallized calcium deposits on tumours, so the determination of higher concentrations of Ca in tumour tissues was expected. However, case U02 underwent chemotherapy treatment before surgery, that could have led to cell death and tissue remodelling.

When comparing normal to tumour tissue, the element K presented significant increase in 4 of the sample pairs, which could be a consequence of the used treatment drugs. The exception is, again, case study U02. On the other hand, regarding case study U03 this was the only element that presented significant differences between normal and tumour tissue. Increase of K and P in breast tissue with tumour, comparing to normal one (but from different individuals) was also observed using Particle Induced X-ray Emission (PIXE) [24] and Neutron Activation Analysis (NAA) [27].

Conversely to what could be expected due to the large pursuit in literature for the association of heavy and transition metals to pathologies[19,28], no significant differences were found for Zn and Fe, with exception of case study B02, where this element was below detection limit (BDL) in normal tissue.

5. Conclusion

We have applied the external standard calibration approach in the quantitative determination of elemental concentration in human tissues. We have constructed several calibration curves with the combination of two sets of CRMs, one set of animal tissues CRMs and other set with plant leaves CRMs. In order to evaluate the difference in the mean-*Z* of the used CRMs, a dependency model of the Rayleigh-to-Compton ratio as a function of the mean Z of the sample

has been developed. We have shown that by combining the two sets, the accuracy in the quantification is highly improved as is shown by the decrease of relative difference of the obtained concentrations of CRM - NIST SRM 1577a Bovine Liver. Moreover, the concentration range to which the curve can be applied was enhanced. The use of standards with a very limited range of concentrations will lead to a calibration graph with large uncertainty on the slope and intercept[1], with higher accuracy in the middle of energy range. This is still a limitation of the external calibration method, but with this methodology the range was extended for all the analysed elements and the uncertainty of the slope and intercept, reduced.

This methodology proved very suitable for the analysis of dark-matrix samples using conventional EDXRF. We have applied this approach to the analysis of a set of paired (normal and tumour) human tissues belonging to females with breast and endometrium carcinoma. Although the number of analysed samples is reduced to draw significant conclusions regarding the genesis of the disease, our quantitative approach rendered an improvement in the accuracy of the elemental determinations in these tissues, allowing to identify significant changes in some light elements, predominantly K. Conversely, no significant changes were determined for Fe and Zn, elements usually investigated in literature.

The gain in accuracy is also advantageous in overcoming the inherent limitation of analysing human tissue samples, the high heterogeneity of elemental distribution.

6. Acknowledgments

This work was partially supported by the research centre grant UID/FIS/04559/2019 to LIBPhys-UNL from the FCT/MCTES/PIDDAC, Portugal. Patrícia M. S. Carvalho acknowledges the support of FCT (Portugal) under contract No. PD/BD/128324/2017. Authors wish to thank REQUIMTE/NOVA School of Sciences and Technology for the ICP-AES analysis.

References

1 B. Z. R. Sitko, in *X Ray spectroscopy*, ed. S. K. Sharma, InTech Open, 2012, pp. 137–162.

2 J. Sherman, *Spectrochim. Acta*, 1955, **7**, 283–306.

3 M. Mantler and N. Kawahara, *Rigaku J.*, 2004, **21**, 17–25.

4 L. Pascolo, I. Venturin, A. Gianoncelli, R. Bortul, G. Zito, E. Giolo, M. Salomé, D. E. Bedolla, M. Altissimo, M. Zweyer and G. Ricci, *Reprod. Biomed. Online*, 2018,

37, 153–162.

5 R. Padilla, P. Van Espen, A. Abrahantes and K. Janssens, *X-Ray Spectrom.*, 2005, **34,** 19-27.

6 S. Pessanha, C. Fonseca, J. P. Santos, M. L. Carvalho and A. A. Dias, *X-Ray Spectrom*., 2018, **47**, 108–115.

7 A. Banas, W. M. Kwiatek, K. Banas, M. Gajda, B. Pawlicki and T. Cichocki, *J. Biol. Inorg. Chem.*, 2010, **15**, 1147–1155.

8 W. M. Kwiatek, A. Banaś, M. Gajda, M. Gałka, B. Pawlicki, G. Falkenberg and T. Cichocki, *J. Alloys Compd.*, 2005, **401**, 173–177.

9 K. Geraki, M. J. Farquharson and D. A. Bradley, *Phys. Med. Biol.*, 2002, **47,** 2327

10 M. E. Poletti, O. D. Gonçalves, C. A. Pérez and S. D. Magalhães, *Radiat. Phys. Chem.*, 2004, **71**, 975–976.

11 M. J. Farquharson and K. Geraki, *X-Ray Spectrom.,* 2004, **33**, 240–245.

12 M. P. Silva, A. Tomal, C. A. Pérez, A. Ribeiro-silva and M. E. Poletti, 2009, **38**, 103–111.

13 C. C. Abnet, B. Lai, Y. L. Qiao, S. Vogt, X. M. Luo, P. R. Taylor, Z. W. Dong, S. D. Mark and S. M. Dawsey, *J. Natl. Cancer Inst.*, 2005, **97**, 301–306.

14 G. Ma and H. C. Allen, *Handbook of Spectroscopy, Volumes 1 and 2 Edited by Günter Gauglitz (University of Tübingen) and Tuan Vo-Dinh (Oak Ridge National Laboratory). Wiley-VCH Verlag GmbH & Co. KGaA: Weinheim. 2003. 1168 pp. $435.00. ISBN: 3-527-29782-0.*, 2004, vol. 126.

15 Z. Uzunoğlu, D. Yilmaz and Y. Şahin, *Radiat. Phys. Chem.*, 2015, **112**, 189–194.

16 I. Antcheva, M. Ballintijn, B. Bellenot, M. Biskup, R. Brun, N. Buncic, P. Canal, D. Casadei, O. Couet, V. Fine, L. Franco, G. Ganis, A. Gheata, D. G. Maline, M. Goto, J. Iwaszkiewicz, A. Kreshuk, D. M. Segura, R. Maunder, L. Moneta, A. Naumann, E. Offermann, V. Onuchin, S. Panacek, F. Rademakers, P. Russo and M. Tadel, *Comput. Phys. Commun.*, 2009, **180**, 2499–2512.

17 M. Morháč, J. Kliman, V. Matoušek, M. Veselský and I. Turzo, *Nucl. Instruments Methods Phys. Res. Sect. A Accel. Spectrometers, Detect. Assoc. Equip.*, 1997, **401**, 113–132.

18 G. D. Ruxton, D. M. Wilkinson and M. Neuhäuser, *Anim. Behav.*, 2015, **107**, 249–252.

19 A. M. Ebrahim, M. A. H. Eltayeb, M. K. Shaat, N. M. A. Mohmed, E. A. Eltayeb and A. Y. Ahmed, *Sci. Total Environ.*, 2007, **383**, 52–58.

20 S. Pessanha, S. Silva, L. Martins, J. P. Santos and J. M. Silveira, *J. Anal. At.*

Spectrom., 2019, **34**, 854-859.

21 A. N. Kadachi and M. A. Al-Eshaikh, *X-Ray Spectrom.*, 2012, **41**, 350–354.

22 *Capability of detection - part 2: Methodology in the linear calibration case - ISO 11843*, London, 2000.

23 Q. Pasha, S. A. Malik, J. Iqbal, N. Shaheen and M. H. Shah, *Biol. Trace Elem. Res.*, 2008, **125**, 30–40.

24 D. O. Olaiya, O. I. Alatise, O. O. Oketayo, O. E. Abiye, E. I. Obianjunwa and F. A. Balogun, *Breast Cancer Basic Clin. Res.*, , DOI:10.1177/1178223419840694.

25 A. Kubala-Kukuś, D. Banaś, J. Braziewicz, S. Góźdź, U. Majewska and M. Pajek, *Spectrochim. Acta - Part B At. Spectrosc.*, 2007, **62**, 695–701.

26 M. Nasiadek, T. Krawczyk and A. Sapota, *Hum. Exp. Toxicol.*, 2005, **24**, 623–630.

27 A. N. Garg, V. Singh, R. G. Weginwar and V. N. Sagdeo, *Biol. Trace Elem. Res.*, 1994, **46**, 185–202.

28 P. Rzymski, P. Niedzielski, P. Rzymski, K. Tomczyk, L. Kozak and B. Poniedziałek, *Fertil. Steril.*, 2016, **105**, 1511-1518.e3.

Tables:

Table 1: Information of the studied cases.

Case	**Age (y.)**	**Tumour**	**Diagnosis**
U01	63	Endometrial cancer	Carcinosarcoma
U02	75	Endometrial cancer	High-grade serous carcinoma with neoadjuvant chemotherapy*
U03	50	Endometrial cancer	Clear cell carcinoma
B01	47	Breast cancer	Invasive lobular carcinoma
B02	64	Breast cancer	Invasive breast carcinoma, no special type

*patient was previously treated with 3 cycles of chemotherapy before surgery

Table 2: Comparison of the three sets of CRMs – animal tissues, plants, and combination of both: Linear regression coefficients of the different calibration curves and significance of the slope in standard error units.

	Linear Regression (slope ± SD) x + (intercept ± SD)							
set of CRMs	P	S	K	Ca	Mn	Fe	Cu	Zn
animal tissues	(240± 40) x + (3990± 830)	(360 ± 860) x -(12000 ± 46000)	(14.2 ± 0.4) x + (1800 ± 300)	(21 ± 4) x - (2500 ± 600)	(1.8 ± 0.2) x -(4 ± 2)	(1.23 ± 0.06) x - (25 ± 4)	(0.80 ± 0.02) x - (4.7 ± 0.5)	(0.79 ± 0.03) x - (8 ± 2)

plants and leaves	(430 ± 50) x + (120 ± 170)	(110 ± 20) x + (700 ± 360)	(14.9 ± 0.4) x + (450 ± 180)	(10.5 ± 0.4) x - (1100 ± 700)	(1.97 ± 0.07) x - (29 ± 6)	(1.2 ± 0.1) x - (11 ± 35)	(1.03 ± 0.09) x -(9 ± 1)	(0.66 ± 0.08) x + (4 ± 4)
both	(410 ± 20) x + (200 ± 100)	(135 ± 5) x + (400 ± 150)	(15.6 ± 0.2) x -(600 ± 150)	(10.8 ± 0.3) x - (1170 ± 90)	(1.75 ± 0.04) x - (3.4 ± 0.6)	(1.23 ± 0.04) x - (25 ± 3)	(0.82 ± 0.02) x - (5.8 ± 0.4)	(0.76 ± 0.02) x - (4 ± 2)
	Significance of the slope							
animal tissues	6	0.4	36	5	9	21	40	33
plants and leaves	9	6	37	26	28	12	11	8
both	21	27	78	36	44	31	41	38

Table 3: Comparison of the elemental concentration (µg/g) obtained for NIST SRM 1577a Bovine Liver using the calibration curves obtained only from animal tissues CRM and all CRM. The relative difference to the certified value is also presented in %.

set of CRMs	Zn		Fe		Cu	
	concentration µg/g	Δ %	concentration µg/g	Δ %	concentration µg/g	Δ %
animal tissues	107 ± 5	13	210 ± 13	8	148 ± 4	7
both	109 ± 3	12	209 ± 9	8	150 ± 4	5
set of CRMs	Mn		Ca		K	
	concentration µg/g	Δ %	concentration µg/g	Δ %	concentration µg/g	Δ %
animal tissues	9 ± 3	6	23 ± 794	81	10450 ± 410	5
both	10 ± 1	3	179 ± 123	48	10100 ± 240	1

Table 4: Limit of Detection (LoD) and Limit of Quantification (LoQ) for all studied elements, calculated by regression analysis of the respective calibration curves.

	P	**S**	**K**	**Ca**	**Mn**	**Fe**	**Cu**	**Zn**
LoD (µg/g)	0.016	0.020	0.575	0.640	4.355	2.006	8.185	12.734
LoQ (µg/g)	0.047	0.060	1.725	1.921	13.065	6.019	24.555	38.202

Figure captions:

Figure 1: X-ray fluorescence spectrum of sample U02. The black line shows the full acquired spectrum, the green dashed line represents the background estimation using the method based on the SNIP clipping algorithm and the red filled spectrum shows the acquired spectrum after background removal. The blue dotted line represents the performed fit to the spectrum after background removal (see text for more details).

Figure 2 : Compton-to-Rayleigh Intensity ratio as a function of the mean-*Z* value of the sample. Black full dots represent the experimental values for the HAp [$Ca_{10}(PO_4)_6(OH)_2$] and boric acid [H_3BO_3] samples. The two different curves show two different fit functions, described in the figure legend, applied to the data represented by the black dots. Green triangles represent the plant CRMs Compton-to-Rayleigh ratio, while red squares represent the animal tissues. For both CRM sets the mean-*Z* is calculated using the fit function represented by the blue curve. The error bars are the quadratic combination of the uncertainty from the numerical integration with the largest deviation between measurements of the same samples.

Figure 3: Plot of the certified Fe concentration values as a function of the Fe Kα intensity divided by the Compton-to-Rayleigh ratio for all considered CRMs. Red squares represent the animal tissue CRMs and green dots represent the plant CRMs. The red curve shows the linear fit for the animal tissue CRMs, the green curve shows the linear fit for the plant CRMs, and the black curve shows the linear fit using all CRMs. For each fit, the 1σ confidence interval, represented by the shaded area with the same color as the respective fit curve, is also shown.

Figure 4: Plot of the certified concentration values of S as a function of the S Kα intensity divided by the Compton-to-Rayleigh ratio for all considered CRMs. Red squares represent the animal tissue CRMs and green dots represent the plant CRMs. The red curve shows the linear fit for the animal tissue CRMs, the green curve shows the linear fit for the plant CRMs, and the black curve shows the linear fit for all CRMs. For each fit, the 1σ confidence interval, represented by the shaded area with the same color as the respective fit curve, is also shown.

Figure 5: Plot of the certified concentration values of K as a function of the K Kα intensity divided by the Compton-to-Rayleigh ratio for all considered CRMs. Red squares represent the animal tissue CRMs and green dots represent the plant CRMs. The red curve shows the linear fit for the animal tissue CRMs, the green curve shows the linear fit for the plant CRMs, and the black curve shows the linear fit for all CRMs. For each fit, the 1σ confidence interval, represented by the shaded area with the same color as the respective fit curve, is also shown.

Figure 6: Comparison of mean elemental concentration for normal and tumor for sample U02. Error bars correspond to one standard deviation of 15 measurements. Significant differences for Wilcoxon Sign rank test are presented with correspondent p-value.

Figure 7: Comparison of mean elemental concentration for normal and tumor for sample B01. Error bars correspond to one standard deviation of 15 measurements. Significant differences for Wilcoxon Sign rank test are presented with correspondent p-value.

Dear editor,

We are very grateful to the reviewers and editorial office for their valuable corrections to our manuscript and we have rewritten the revised version manuscript to comply with these new suggestions.

The answers to the reviewer queries are detailed below.

We hope that this improved version of the manuscript can be now considered for publication in JAAS.

Best regards,

On behalf of the remaining authors,

Sofia Pessanha

Referee 3

Comments to the author:

The authors answered the reviewers' questions and inserted part of these clarifications in the final manuscript. I believe that this decision by the authors left the manuscript better, in conditions to be published. I draw your attention that there is a mistake in the numbering of the Figures. I have the impression that the authors wished they should just call Figure 1 and Figure 2, or Figure 1 (a) and (b). Thus, the numbering of the other figures must change. I suggest to the authors to open a session of supplementary material, in which Figures 6 to 11 and Figure 1, used in the answer to reviewer 3 - Comparison of the concentration values of P, K, and Zn in sample B01 Normal, determined by XRF and ICP-AES analysis, can be moved.

We thank the referee for recognizing our effort and for noticing the mistake in the figures' labelling. In fact, there has been some confusing due to the insertion of Figure 1a.

As suggested, we have opened an ESI, where figures 1, 6, 8, 10 and the comparison with ICP-AES analysis was included. Nevertheless, we have kept figures 7 and 9 (now figures 6 and 7) in the manuscript. We believe that at least these two figures should stay in the manuscript to illustrate the discussion in section 4. On one hand, several aspects concerning the quantification of case study U02 are addressed, on the other hand, case study number B01 was analysed with ICP-AES and the results from both analytical procedures were compared. Section 4 has been altered to accommodate these changes, and we have included a brief mention of the ICP-AES analysis:

"Sample B01 was also analysed destructively using Inductively Coupled Plasma – Atomic Emission Spectroscopy (ICP-AES) and the results are within the obtained order of magnitude for elements P, K and Zn (Fig.S5). "

All figures' labels have been corrected overall the manuscript. References to the figures that were moved to ESI have been also changed in the text.

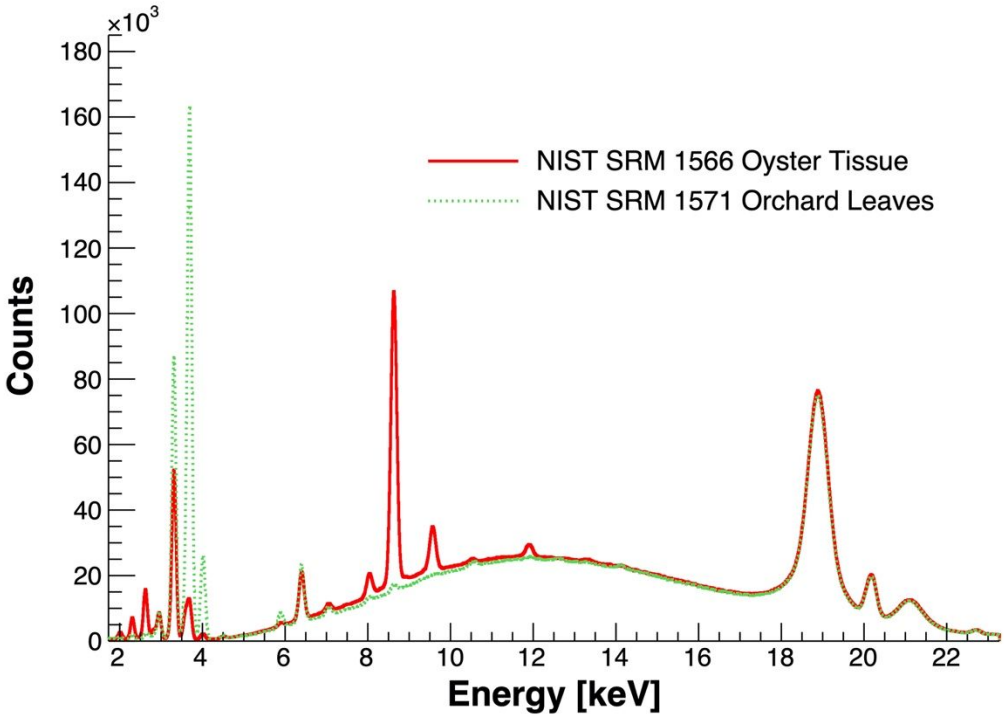

Figure S1: Comparison of the X-ray fluorescence spectra obtained for reference materials NIST SRM 1566 Oyster Tissue (red full curve) and NIST SRM 1571 Orchard Leaves (green dashed curve).

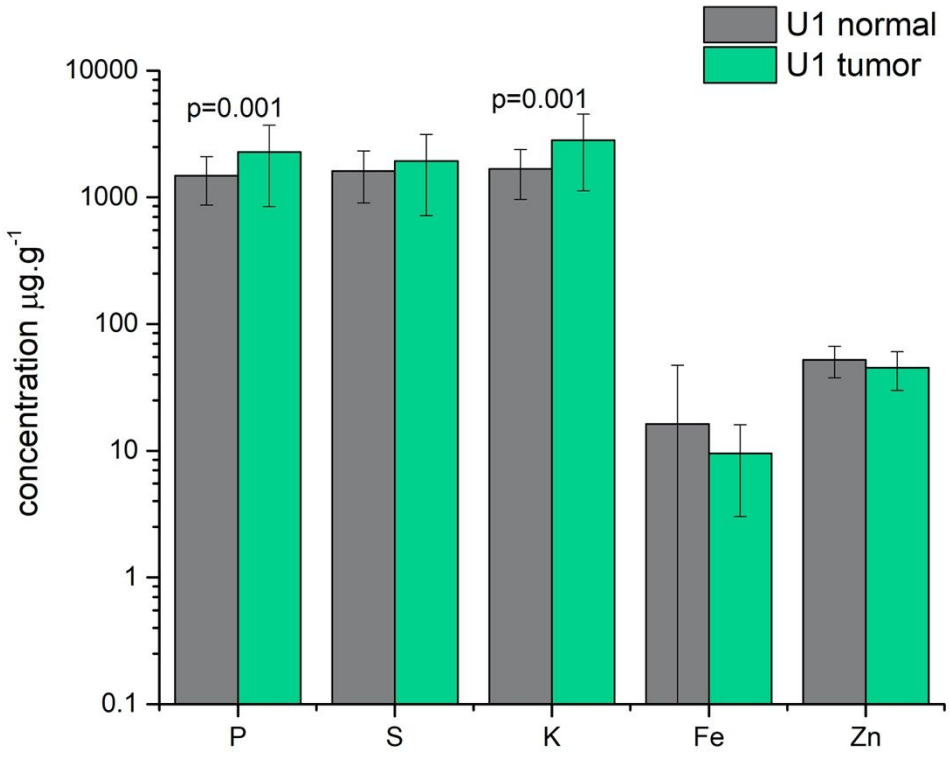

Figure S2: Comparison of mean elemental concentration for normal and tumor for sample U01. Error bars correspond to one standard deviation of 15 measurements. Significant differences for Wilcoxon Sign rank test are presented with correspondent p-value.

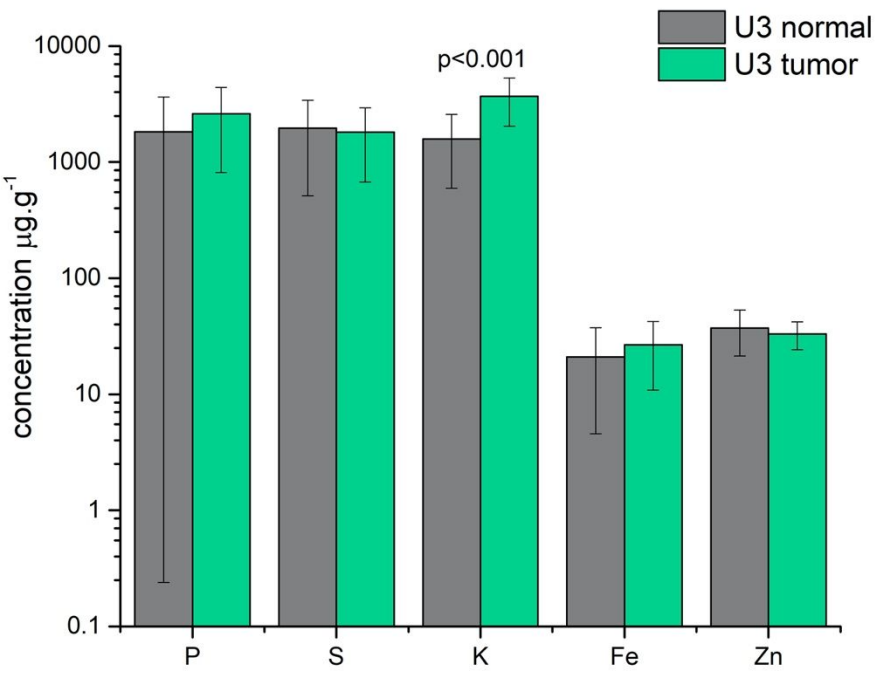

Figure S3: Comparison of mean elemental concentration for normal and tumor for sample U03. Error bars correspond to one standard deviation of 15 measurements. Significant differences for Wilcoxon Sign rank test are presented with correspondent p-value.

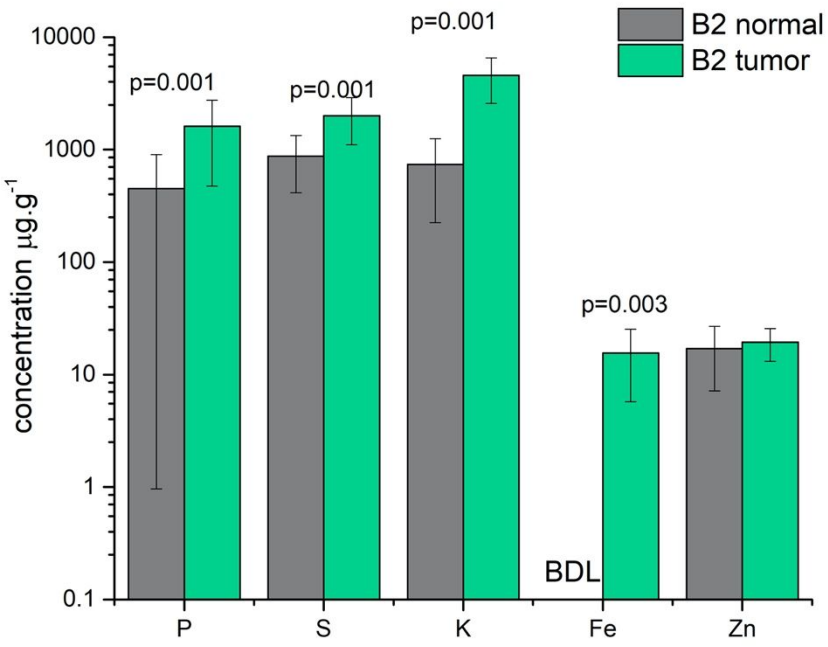

Figure S4: Comparison of mean elemental concentration for normal and tumor for sample B02. Error bars correspond to one standard deviation of 15 measurements. Significant differences for Wilcoxon Sign rank test are presented with correspondent p-value.

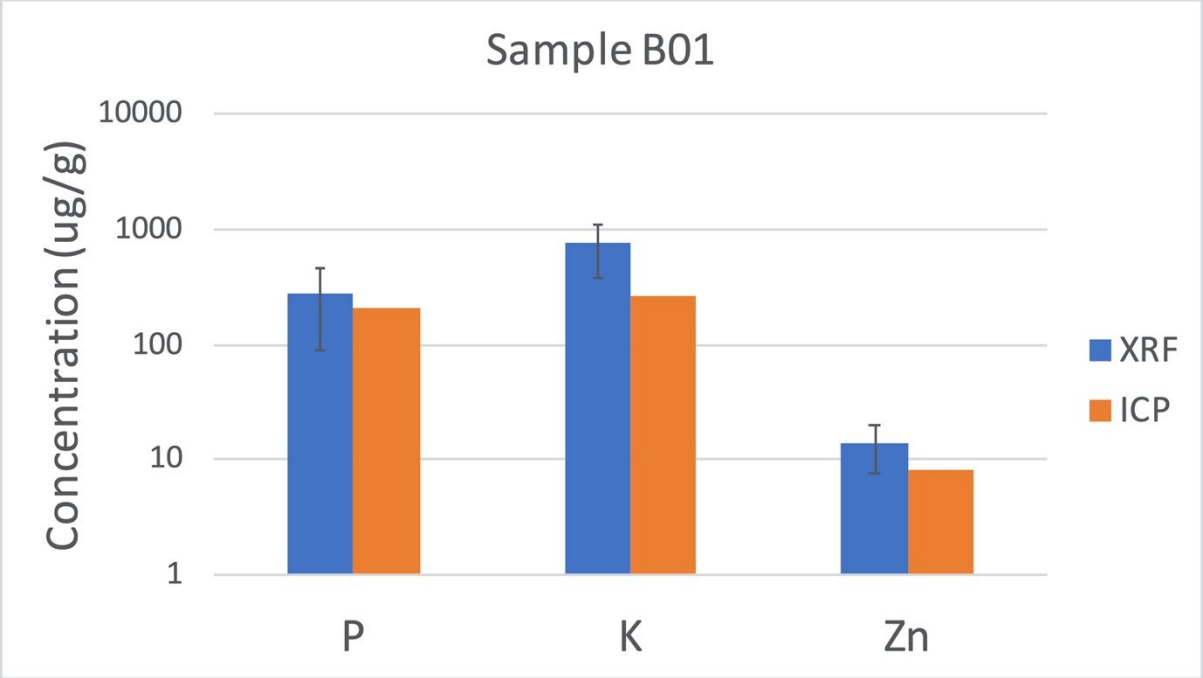

Figure S5: Comparison of the concentration values of P, K and Zn in sample B01 Normal, determined by XRF and ICP-AES analysis. ICP measurements were performed using Horiba Jobin-Yvon, France, Ultima, model equipped with a 40.68 MHz RF generator, Czerny-Turner monochromator with 1.00 m (sequential).

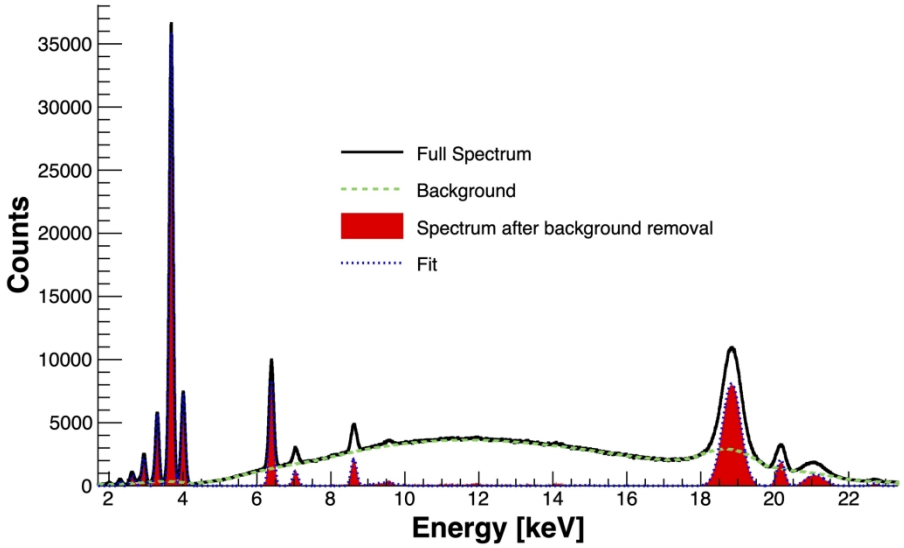

199x119mm (300 x 300 DPI)

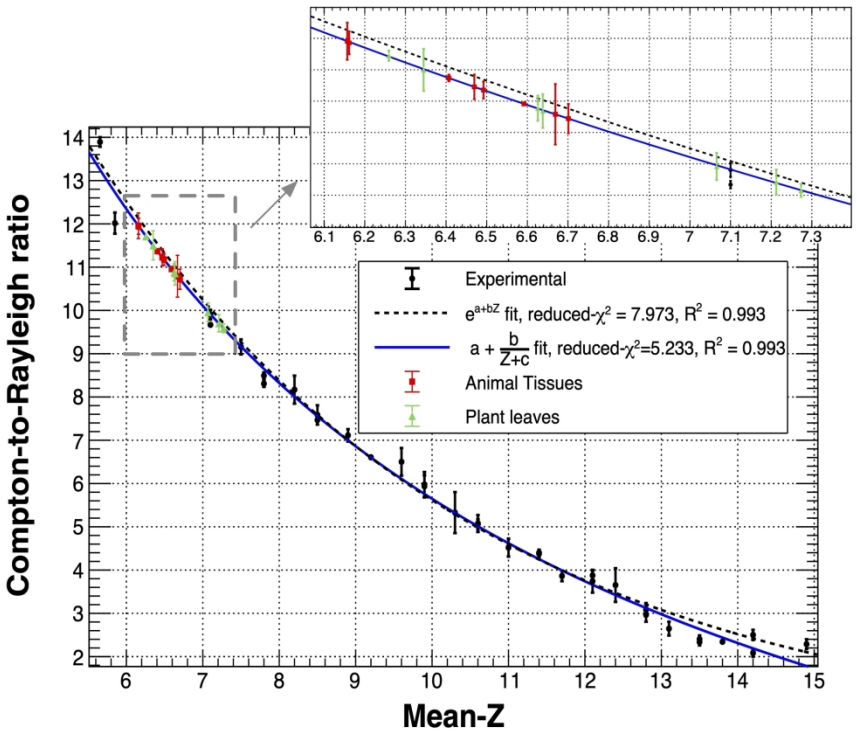

200x147mm (300 x 300 DPI)

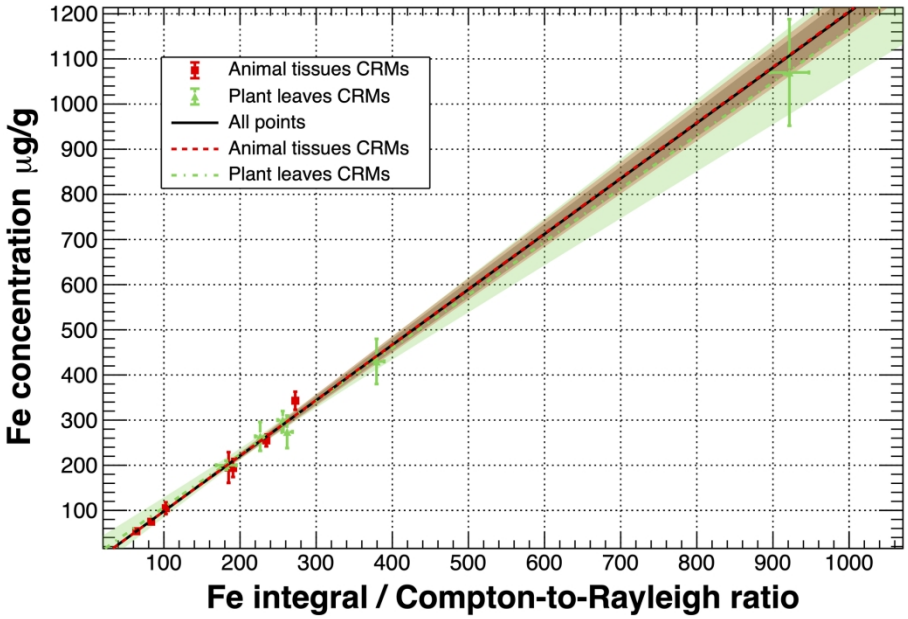

199x135mm (300 x 300 DPI)

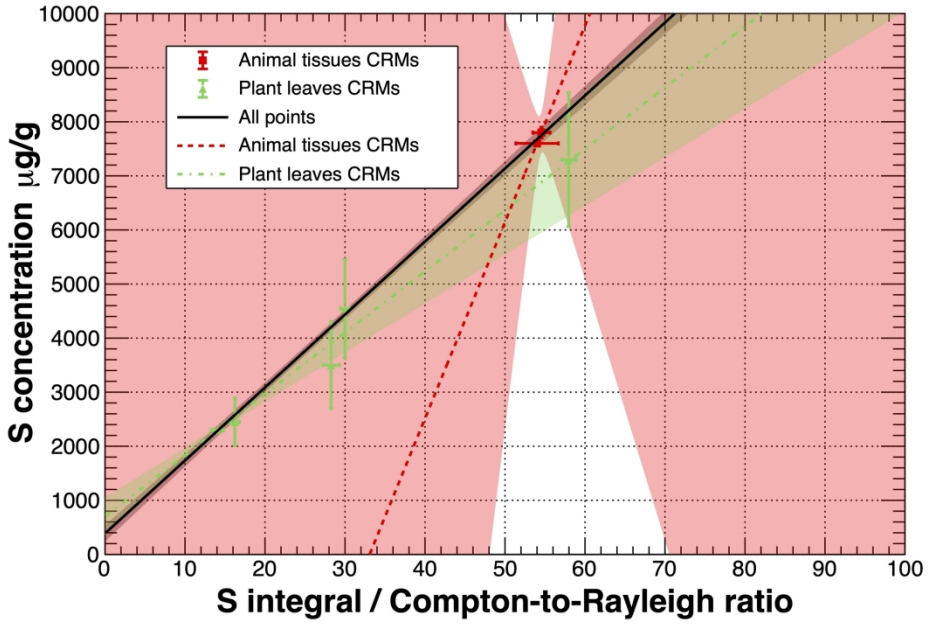

199x135mm (300 x 300 DPI)

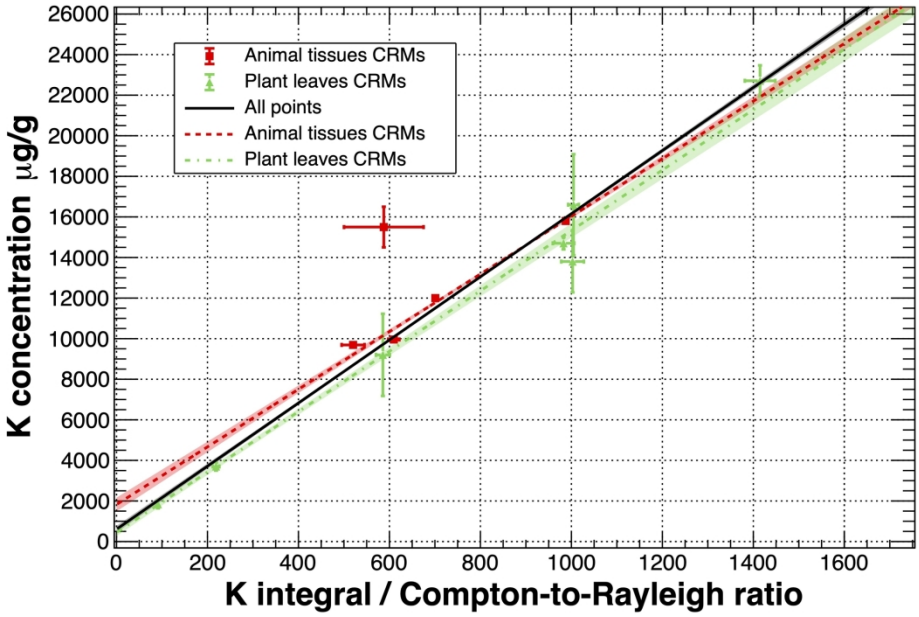

199x135mm (300 x 300 DPI)

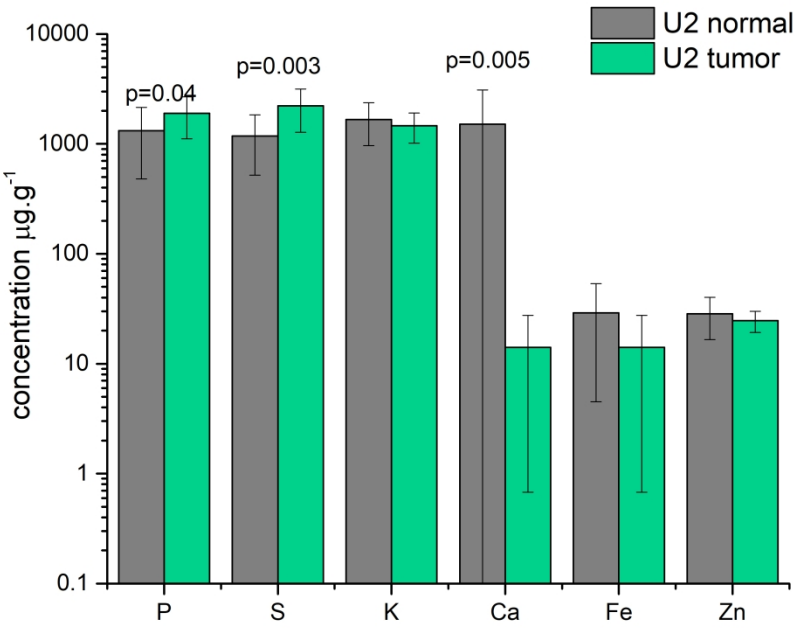

272x208mm (300 x 300 DPI)

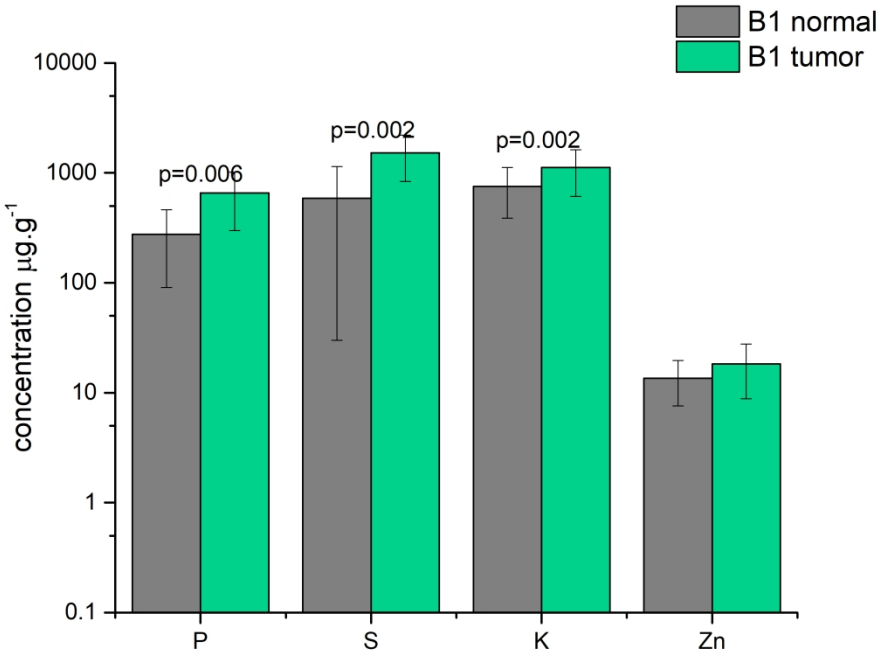

272x208mm (300 x 300 DPI)